Boris B. Straumal[a,b], Sergei A. Polyakov[a–c], Ewald Bischoff[b], Eric J. Mittemeijer[b,c]
[a] Institute of Solid State Physics, Russian Academy of Sciences, Chernogolovka, Russia
[b] Max Planck Institute of Metals Research, Stuttgart, Germany
[c] Institute for Physical Metallurgy, University of Stuttgart, Stuttgart, Germany

Grain boundary faceting close to the $\Sigma 3$ coincidence misorientation in copper

Dedicated to Prof. Dr. Helmut Mehrer on the occasion of his 65th birthday

The faceting of a cylindric tilt grain boundary (GB) in Cu bicrystal has been studied. The crystal lattices of both grains give rise to a superlattice called coincidence site lattice (CSL) with inverse density of coincidence sites $\Sigma = 3$. The $(100)_{CSL}$, $(210)_{CS}$L, $(130)_{CSL}$ facets and the non-CSL 82°9*R* facet develop upon annealing at 0.95 T_m, where T_m is the melting temperature. The ratio of GB energy σ_{GB} and surface energy σ_{sur} of the specimen was measured applying atomic force microscopy from the profile of the GB thermal groove formed upon additional annealing. The influence of deviation from the exact coincidence misorientation θ_Σ, $\Delta\theta = |\theta - \theta_\Sigma|$, has been studied on the basis of electron backscattering diffraction patterns. The Wulff–Herring diagrams were constructed using measured σ_{GB}/σ_{sur} values, revealing stable and metastable GB facets. T_m is lower than the roughening temperature for the $(100)_{CSL}$ and 9*R* facets facets in Cu.

Keywords: Grain Boundaries; Faceting; Misorientation dependence; Stability diagrams

1. Introduction

Faceting is a well documented phenomenon known both for surfaces and interfaces, particularly, grain boundaries (GBs) [1–4], that attracts more and more attention. Thus, the faceting of semiconductor surfaces permits to form self-assembled nanoscale gratings, fine one-dimensional structures like quantum wires, ordered arrays of quantum dots, etc. [1, 3, 5]. Surface faceting is important for epitaxial growth, chemical etching, and catalysis. The transition from rough to faceted GBs can induce abnormal grain growth in metals [6] or influence significantly the properties of ceramics [7]. Faceting can be considered as a phase transition when the original surface or original GB dissociates into flat segments whose energy is less than that of the original surface or GB. GB faceting proceeds only close to the so-called coincidence misorientations. In this case the lattices of both grains form the coincidence site lattice (CSL) characterized by the parameter Σ (inverse density of coincidence sites). In most cases the GB facets are parallel to the CSL planes with high density of coincidence sites. It has been shown [8] that the GBs close to coincidence misorientations θ_Σ possess special (CSL derived) structure and properties in limited ranges of temperature T and misorientation θ with respect to θ_Σ. By increasing $\Delta\theta = |\theta - \theta_\Sigma|$ and T the phase transition "special GB → general GB" proceeds and the GB looses its special (CSL derived) structure and properties [9]. The higher Σ the lower are the values of temperature and $\Delta\theta$ at which a GB looses its special structure and properties, because for the CSLs of low Σ the depth of the profile of GB energy versus misorientation is more pronounced than for CSLs of high Σ [10]. Recently it was observed that similar phenomena occur also for GB facets lying in different CSL planes [11]. At high temperature only the facets with the highest density of coincidence sites appear, and with decreasing temperature the number of facet types increases, i. e. the facets with smaller density of coincidence sites and consequently less deep energetic minima appear.

The influence of a small deviation $\Delta\theta$ from the exact coincidence misorientation θ_Σ on GB faceting has not been studied until now. Such an analysis is provided here. For this purpose the most closely packed CSL boundary was chosen, namely the $\Sigma = 3$ coincidence GB (twin GB), in copper. Twin GBs form the majority of special GBs in materials as copper and stainless steel and influence pronouncedly their properties [6, 12].

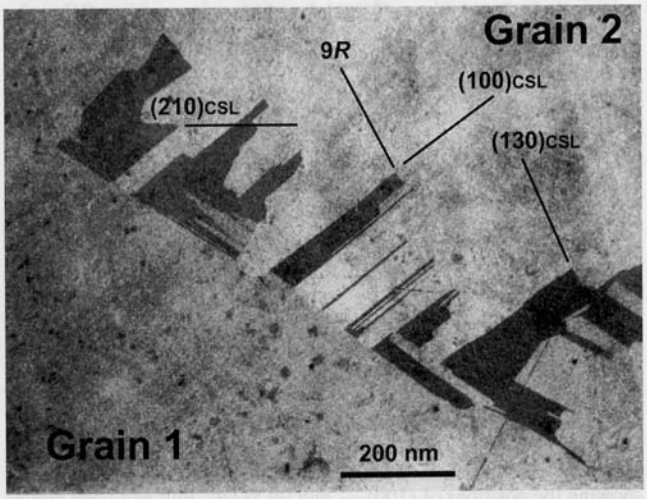

Fig. 1. Micrograph of twins which had developed between grain 1 and grain 2 with $\Sigma 9$ misorientation during growth of the bicrystal. The common [110] tilt axis is perpendicular to the plane of the micrograph.

2. Experimental

For the investigation of GB faceting, a cylindrical Cu bicrystal with an island (inner) grain was grown by the Bridgman technique from Cu of 99.999 wt.% purity. The grain 1 in this bicrystal is completely surrounded by the grain 2 forming the $\Sigma 9$ <110> tilt GB. The {111}/{115} inclination of the $\Sigma 9$ GB is unstable against the dissociation reaction: $\Sigma 9 \rightarrow \Sigma 3 + \Sigma 3$. Therefore, elongated twins (Fig. 1) with well-developed $\Sigma 3$ GBs appear during the growth of the bicrystal, instead of $\{111\}_1/\{115\}_2$ [or $(110)_{\Sigma 9CSL}$] facets (the subscripts 1 and 2 correspond to the grains 1 and 2) [11]. The <110> axes in both grains are parallel to the growth axis. Therefore, the $\Sigma 3$ <110> tilt GB in the cylindrical sample with <110> cylinder axis contains all crystallographically possible inclinations. The section of $\Sigma 3$ CSL perpendicular to the {110} tilt axis with indication of the $(100)_{CS}L$ [or $\{111\}_1/\{111\}_2$] and 9R facets is shown in Fig. 2a.

A natural variation in misorientation angle θ occurs for the $\Sigma 3$ twin GBs in the bicrystal. This is due to the fact that the bicrystals grown by the Bridgman technique are not completely ideal. Subgrain boundaries are always present in the single- and bicrystals due to the instability of the growth process. Since GB energy and misorientation θ can be measured accurately and locally by atomic force microscopy (AFM) and electron backscattering diffraction (EBSD), respectively, this natural θ spread (about 1°) was used here to investigate the influence of the deviation of θ from exact coincidence misorientation θ_Σ on the GB faceting of $\Sigma 3$ twin GBs.

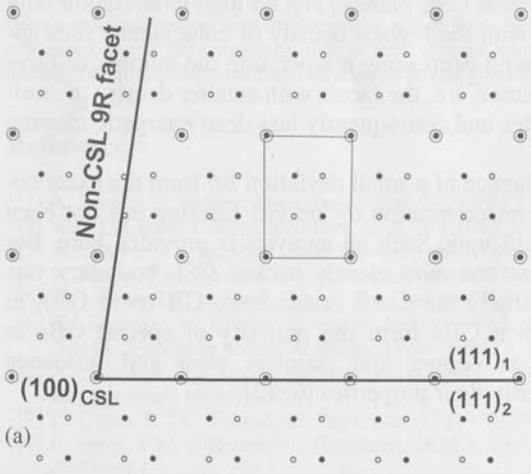

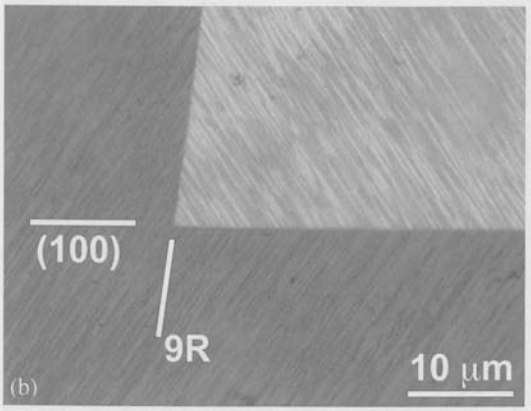

Fig. 2. (a) Section of the $\Sigma 3$ CSL perpendicular to the <110> tilt axis showing the positions of $(100)_{CSL}$ and 9R facets. Full and open circles mark the atoms of misoriented lattices 1 and 2. Double circles mark the sites of CSL. (b) Micrograph of the intersection of $(100)_{CSL}$ and 9R facets after annealing at 1293 K.

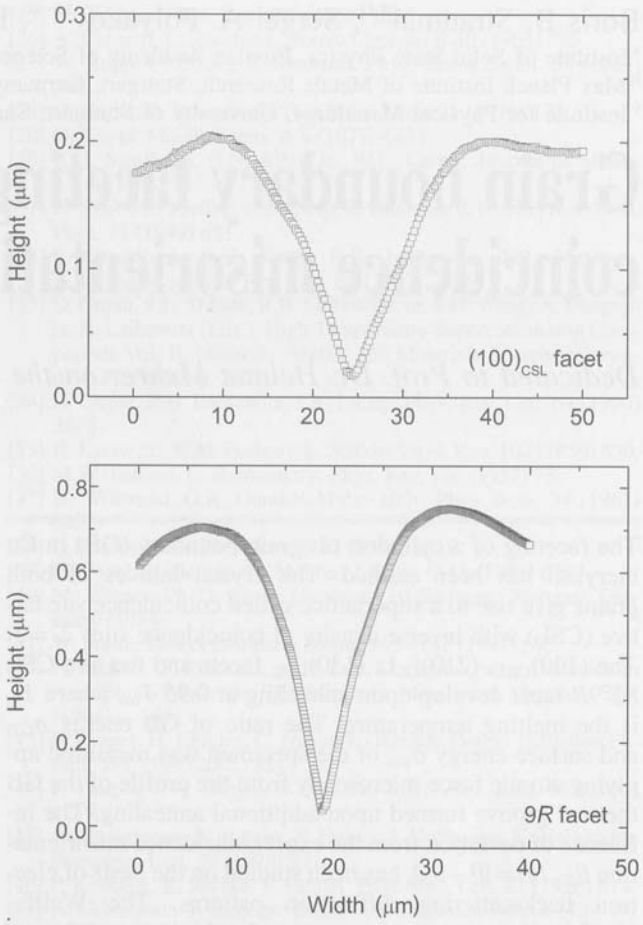

Fig. 3. Thermal GB groove profiles as measured by AFM for $(100)_{CSL}$ and 9*R* facets.

2.5 mm thick platelets were cut from the grown bycrystal perpendicularly to the growth axis. The platelets were ground with 4000 SiC paper and polished with 3 and 1 μm diamond paste. This was followed by an anneal in 80 % Ar + 20 % H_2 gas mixture at a pressure of 2×10^4 Pa at a temperature of 1293 K for 48 h. During the annealing the GB migrates slowly towards the centre of the bicrystal and facets develop in correspondence with the annealing temperature. The annealed samples were etched in a 50 vol.% HNO_3 aqueous solution. The GB shape and the geometry of the facets were analyzed and photographed in polarized light in bright and dark field with the aid of a Zeiss Axiophot optical microscope.

The sample was then carefully repolished and annealed 48 h once again at 1293 K in order to form GB thermal grooves. The profiles of the formed GB thermal groove were analysed with the aid of the Topometrix 2000 Explorer AFM operating in the contact mode. The typical field analyzed with the aid of AFM had a size of 50×50 μm containing 500×500 pixels. For the analysis of all GBs 10 neighbouring groove profiles were used to obtain a mean profile. Such mean groove profiles for GB facets of low energy [$(100)_{CSL}$ facet] and of high energy (9*R* facet) are

shown in Fig. 3. The ratio of GB energy σ_{GB} and surface energy (of the specimen with GB groove) σ_{sur} was calculated using the measured value of the GB groove tip angle. For the determination of the groove angle not only the groove tip but the full groove profile was used [13]. The two sides of the groove profile were approximated separately starting from the maxima on the groove profile. As demonstrated previously, the finite radius of the AFM needle does not allow to measure correctly the profile close to the tip of the groove. Therefore, the approximated "left" and "right" halves of the groove profile were extrapolated down to the intersection point, on the basis of a physical model of the groove profile. This procedure allows one to determine the coordinates of the "true" groove tip which is positioned lower than the tip observed by the AFM. Polynomials of 1^{st}, 2^{nd}, 4^{th}, 6^{th}, and 8^{th} order were compared. The transition from 1^{st} to 2^{nd} to 4^{th} order improves the results drastically. Further extension of the polynomials does not change the results. Therefore, polynomials of 4^{th} order were used for the approximation. The derivatives for both halves of the groove profile were determined in the intersection point. Their sum delivers the true value of the groove angle [14].

The local misorientation was determined at the same locations where the GB energy was measured using a scanning electron microscope (SEM) equipped with an EBSD unit. The EBSD patterns were evaluated using a commercially available system (OIM^{TM}, by TSL) capable of automatic pattern indexing. The accuracy in misorientation determination was about $\pm 0.2°$.

3. Results

At $T = 1293$ K (0.95 T_m, i. e. very close to the melting temperature) the $\Sigma 3$ GB exhibits two facets. The crystallographic relation of both facets is shown in Fig. 2a. The energy of the symmetric $\Sigma 3$ twin GB [or $\{111\}_1/\{111\}_2$ facet, or $(100)_{CSL}$ facet] is very low. The second close packed CSL plane is $\{211\}_1/\{211\}_2$ [or $(010)_{CSL}$] facet, the so-called asymmetric twin GB. The angle between the facets $(100)_{CSL}$ and $(010)_{CSL}$ is 90°. The occurence of such facets has been well documented for Al, Au, $AuCu_3$, and Ge [15–18]. The typical rectangular twin plates bounded by $(100)_{CSL}$ and $(010)_{CSL}$ facets have been observed, for example for Au thin films [16]. However, such twin plates in Cu and Ag do not show a rectangular shape. The end facet forms an angle of 82° with the $\{111\}_1/\{111\}_2$ or $(100)_{CSL}$ facets [19, 20]. Transmission electron microscopy (TEM) studies revealed that this 82° facet has a so-called 9*R* structure forming a very thin plate of bcc GB phase in the fcc matrix [21–23]. Such $(100)_{CSL}$ and 82° 9*R* facets are clearly seen for the $\Sigma 3$ twin plate in our samples (see Figs. 1a and 2b).

Some short $(210)_{CSL}$ and $(130)_{CSL}$ facets can also be discerned. The length of these facets is only a few per cent of the overall length of $\Sigma 3$ GBs. To the best of our knowledge, such $(210)_{CSL}$ and $(130)_{CSL}$ facets for the $\Sigma 3$ GB in Cu were never reported before.

EBSD measurements were performed in order to determine the deviation from the exact coincidence misorientation corresponding to the $\Sigma 3$ <110> tilt GB in the Cu bicrystal. From these measurements, made at different locations along the GB, it followed that the maximal measured $\Delta\theta$ is only about 1°. The maximal value reported for $\Delta\theta$ in the literature for $\Sigma 3$ GBs is about 5° [8, 24]: for $\Delta\theta \leq 5°$

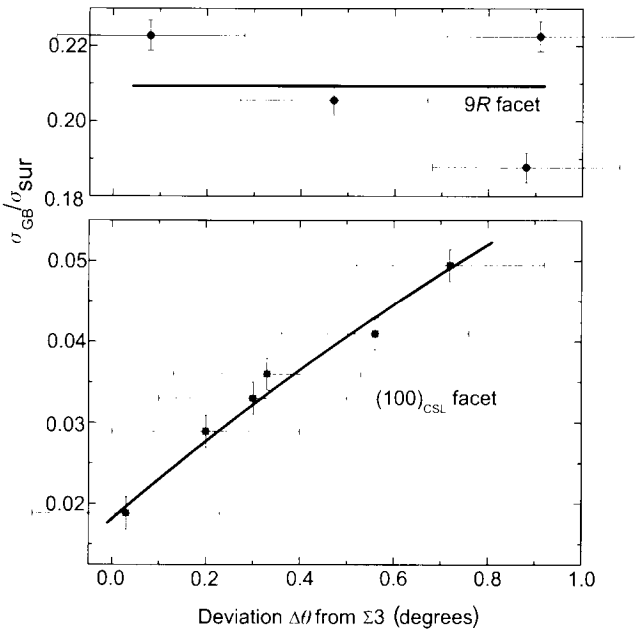

Fig. 4. Dependence of σ_{GB}/σ_{sur} on deviation $\Delta\theta$ from the exact $\Sigma 3$ coincidence misorientation for the 9*R* facet (top) and $(100)_{CSL}$ facet (bottom).

$\Sigma 3$ (twin) GBs still conserve their special structure and properties.

The measured dependences of σ_{GB}/σ_{sur} ratio on the deviation $\Delta\theta$ from the exact $\Sigma 3$ coincidence misorientation for both the 9*R* facet and the $(100)_{CSL}$ facet are shown in Fig. 4. The σ_{GB}/σ_{sur} ratio for the $(100)_{CSL}$ facet increases from the very low value of 0.02 close to the exact coincidence misorientation to 0.05 for $\Delta\theta \cong 0.7°$. The σ_{GB}/σ_{sur} ratio for the 9*R* facet is much higher and maintains a practically $\Delta\theta$ (for $\Delta\theta < 1°$) independent value of about 0.21.

4. Discussion

GBs close to the exact coincidence misorientation θ_Σ contain portions of the ideal GB, corresponding to $\Delta\theta = 0$, separated by a network of intrinsic GB dislocations (IGBDs) [25]. These IGBDs allow these GBs to conserve the low-energy coincidence structure as well as possible. The energy of a GB with a network of IGBDs can be described by Read's equation [26, 27] provided that the lattice Burgers vector b is replaced by the Burgers vector of the IGBDs $b_\Sigma = b\Sigma^{-0.5}$ [25]:

$$\sigma_{GB} = \sigma_\Sigma(1 - 4\Delta\theta) + \sigma_0 \Delta\theta (A - \ln \Delta\theta) \quad (1)$$

where σ_Σ is the GB energy at exact coincidence angle θ_Σ. The factor $(1-4\Delta\theta)$ reflects the fact that the total length of IGBD cores with diameter $\sim 4b_\Sigma$ has to be subtracted from the overall GB length, and

$$\sigma_0 = \mu b_\Sigma/[4\pi(1-\nu)] \quad (2)$$

and

$$A = \{[4\pi(1-\nu)\, E_c]/\mu b_\Sigma^2\} - \ln (r_0/b_\Sigma) \quad (3)$$

where ν is the Poisson ratio, μ is the elastic shear modulus, r_0 is the core radius of the IGBD and E_c is energy per unit length of dislocation line core. The observed linear increase

of σ_{GB}/σ_{sur} [here σ_{GB} represents the overall GB energy: the energy of the GB that is "ideal" ($\Delta\theta = 0$) and the energy of the part of the GB with a network of IGBDs obeying Eqs. (1) to (3)] with increasing $\Delta\theta$ qualitatively agrees with Eq. (1) (Fig. 4).

An inclusion of one phase can be in thermodynamic equilibrium within a second phase (matrix). Then the shape of the inclusion is determined by the free energy minimum for the creation of the unavoidable interfacial boundary [28–30]. If the GB energy for both coexisting phases is isotropic (e. g. fluids), the shape of the inclusion is spherical. If one or both of the coexisting phases is crystalline, the GB energy is generally anisotropic and interfaces of specific orientations are preferred over others. Then the "equilibrium crystal shape" (ECS) of the inclusion is nonspherical.

The problem of finding the ECS for a "free" crystal (i. e. in an isotropic medium) was first considered by Wulff [31, 32]. He proposed the following construction (see. Fig. 5a). The interface (surface) free energy per unit area $f(\boldsymbol{m})$ as a function of interface orientation is presented in a polar plot (Wulff plot, also called γ-plot). In such a plot the interface energy, f, is indicated by the length of a vector, $\boldsymbol{m}$, drawn from the centre point in a direction representing the direction of the normal to the interface considered. The equilibrium crystal shape (ECS) is then given by the interior envelope of the family of perpendicular planes drawn through the end points of the radius vectors $\boldsymbol{m}$. The ECS is also indicated by $r(\boldsymbol{h})$, where $\boldsymbol{h}$ represents the facet orientation, relating to the crystal axes. The $r(\boldsymbol{h})$, obtained by the procedure as discussed above, can be drawn in the Wulff plot.

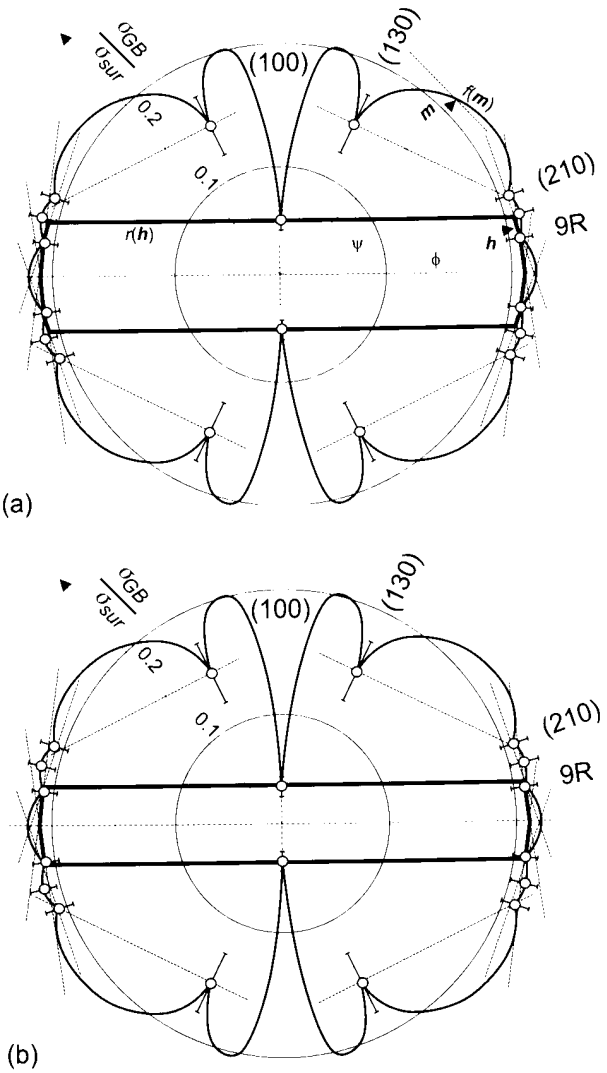

Fig. 5. Wulff–Herring GB energy plot, $f(\boldsymbol{m})$, and resulting ECS, $r(\boldsymbol{h})$, in plane section perpendicular to the <110> tilt axis for the $\Sigma 3$ GBs in Cu at 1293 K for deviations $\Delta\theta$ from exact coincidence misorientation that (a) are relatively large ($\Delta\theta = 0.75°$) and (b) relatively small ($\Delta\theta = 0.05°$). Open data points represent the GB energy (σ_{GB}) for various facets measured with AFM. The large circles mark the values (σ_{GB}/σ_{sur}) = 0.1 and 0.2. ψ and φ are angular variables which indicate interfacial orientation ($\boldsymbol{m}$) and crystal shape ($\boldsymbol{h}$), respectively (see text).

Usually in the literature the situation was considered, both theoretically and experimentally, where only one phase (namely the "inclusion") is crystallographically anisotropic and the second phase is isotropic (gas, liquid); see above description of Wulff's plot. This resembles the description of the equilibrium shape for the surface of crystals. What happens when both "matrix" and "inclusion" are crystalline and crystallographically anisotropic? Grain boundaries representing the interfaces between two identical but misoriented lattices represent the simplest example of this case. The approach developed originally for the description of the ECS of a "free" crystal can then also be used for such bicrystals. Evidently, in the case of grain boundaries, as compared to free surfaces (FSs), the volume of the "inclusion" is not constant. In case of GBs, the derived ECS refers to a slowly growing or slowly dissolving crystal.

On the basis of the σ_{GB}/σ_{sur} results for the observed facets the Wulff–Herring plot is shown in Fig. 5a for the $\Sigma 3$ GBs at 1293 K for relatively large $\Delta\theta$ (i. e. $\Delta\theta = 0.75°$). A similar Wulff–Herring plot is shown in Fig. 5b for the $\Sigma 3$ GBs at 1293 K for relatively low $\Delta\theta$ ($\Delta\theta \sim 0.05°$). Evidently, the very low energy of the coherent $(100)_{CSL}$ facets governs the platelet-like shape of twins in Cu. The metastable nature of the subordinate $(210)_{CSL}$ and $(130)_{CSL}$ facets is clearly seen in Fig. 5b. The possible presence of a $(210)_{CSL}$ facet (see Fig. 5a) and of a $(130)_{CSL}$ facet is due to the existence of local GB energetic minima in the Wulff–Herring plot, but as follows from Fig. 5b, these local minima are not deep enough to allow the presence of the corresponding facets in the resulting ECS, provided that the $(100)_{CSL}$ facets are of sufficiently low energy. Upon increasing $\Delta\theta$ the opposite $(100)_{CSL}$ planes (faces) of the ECS move away from each another, and beyond $\Delta\theta \sim 0.6°$ the $(210)_{CSL}$ facet appears in the ECS (Fig. 5a).

An extreme case of ECS is a perfectly faceted shape (polyhedron), consisting of strictly planar faces (facets) joining at sharp edges. Rounded shapes can also occur exhibiting a smoothly curved appearance lacking both facets and edges. At $T = 0$ K the ECS is perfectly faceted. At $T > 0$ K, curved interfacial regions may appear in addition to planar regions (facets) [29, 30]. As T increases, the facets shrink and eventually disappear [28], each facet at its own characteristic roughening ("faceting") temperature $T_R(\boldsymbol{h})$ [33]. At sufficiently high temperature the ECS becomes smoothly rounded everywhere (unless, of course, the system first undergoes a bulk phase change, such as melting).

The $(100)_{CSL}/82°9R$ corners of the twin plates, as observed in the current work, are sharp, according to the light microscopical analysis (see Fig. 2b). Yet, AFM revealed a minor rounding at the edge with an extension less than 1 μm. It has been shown [34, 35] that the intersections of

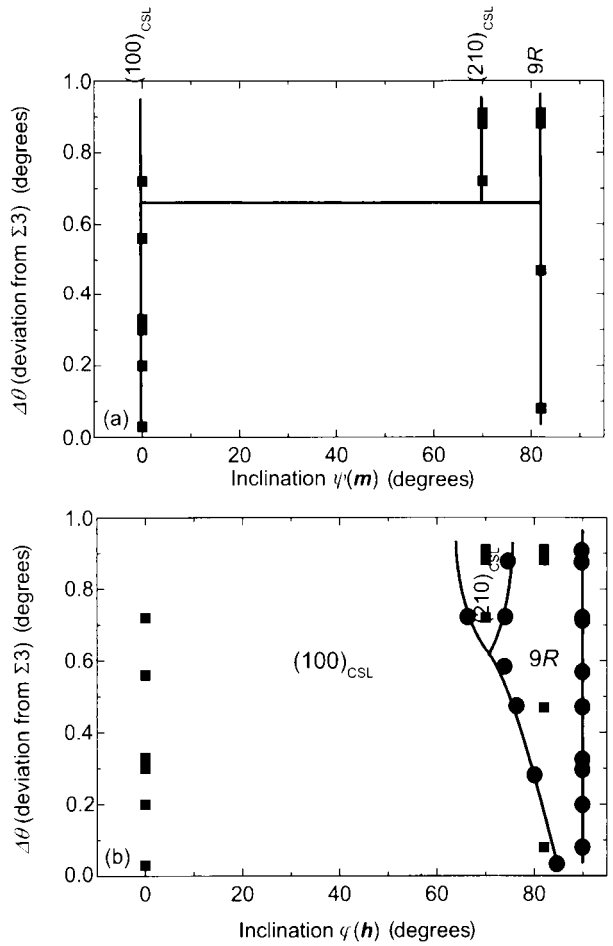

Fig. 6. (a) ($\Delta\theta$, ψ) and (b) ($\Delta\theta$, φ) interface stability diagrams for $\Sigma 3$ <110> tilt GBs in Cu plotted according to the approach [29, 30]. ψ and φ are angular variables which indicate the interface orientation ($\boldsymbol{m}$) and the crystal shape ($\boldsymbol{h}$), respectively, in a plane section of the full three-dimensional ECS which is perpendicular to the <110> tilt axis. (a) The ($\Delta\theta$, ψ) diagram shows the locus of cusps in the Wulff plot. (b) The ($\Delta\theta$, φ) diagram presents the angular outline of the faceted areas of equilibrium GB shape.

facets in principle cannot be ideally sharp even well below the T_R. Hence, it can be concluded that the roughening temperature T_R for $(100)_{CSL}$ and $9R$ facets is higher than the melting temperature T_m (annealing temperature 1293 K = $0.95T_m$). Upon decreasing the annealing temperature new facets may appear in the ECS of $\Sigma 3$ GB, as had been shown in our previous work [4]. All observed corners between facets are sharp, according to the light microscopic analysis. Hence, these new facets appear at the originally sharp, now degenerated edges (corners) between the already existing facets and not at rough rounded GB-like surface facets as observed in Pb, Au or He [36–41].

A decrease of temperature thus plays a qualitatively similar role as an increase of $\Delta\theta$. Stability diagrams for the $\Sigma 3$ GB facets are shown in Fig. 6 according to the approach proposed for ECS in [29, 30]. Instead of the temperature (cf. Fig. 2 in [4]) the deviation from exact coincidence misorientation, $\Delta\theta$, is adopted as ordinate (cf. above discussion). These diagrams can be constructed from Wulff plots, as shown in Fig. 5, for a series of $\Delta\theta$ values. The first diagram, ($\Delta\theta$, ψ) diagram, shows which facets occur as a function of $\Delta\theta$ and reveals that the crystallographic orientations of the occurring facets with respect to each other remain fixed: rough rounded GB like facets (see above discussion) do not occur. The areas between the vertical lines in Fig. 6a can be considered as "two-phase" equilibria between two GB facets. The second diagram, ($\Delta\theta$, φ) diagram, shows which facets bound the ECS as a function of $\Delta\theta$ and which angular extension, as expressed by the angle φ (see Fig. 5a), the various facets in the ECS have. With increasing $\Delta\theta$ the $9R$ range in Fig. 6b becomes broader at the cost of the $(100)_{CSL}$ range. At $\Delta\theta = 0.6°$ the new $(210)_{CSL}$ facet appears between the $(100)_{CSL}$ and $9R$ ranges.

5. Conclusions

1. The cylindrical $\Sigma 3$ <110> tilt GB in a Cu bicrystal, presenting all crystallographically possible inclinations with respect to the <110> tilt axis, becomes faceted upon annealing at $0.95T_m$.
2. The $(100)_{CSL}$, $(210)_{CSL}$, $(130)_{CSL}$ facets and the non-CSL 82°$9R$ facet are observed.
3. Wulff–Herring plots, constructed on the basis of GB energy measurements for the various facets (relative to the surface energy; on the basis of thermal groove profile measurement by Atomic Force Microscopy), for various values of the deviation from exact coincidence misorientation, $\Delta\theta$ (measured from local Electron Back Scattering Diffraction patterns), for the first time allowed determination of the equilibrium crystal shape (ECS) as a function of $\Delta\theta$.
4. For small values of $\Delta\theta$ the $(100)_{CSL}$ and $9R$ facets are stable. Upon increasing $\Delta\theta$ the, $(210)_{CSL}$ ($\Delta\theta > 0.6°$) and $(130)_{CSL}$ ($\Delta\theta > 1°$) facets appear in the ECS.
5. No rough edges (corners) between $(100)_{CSL}$ and $9R$ facets were observed, implying that T_m is lower than the roughening temperature for these facets in Cu.
6. An increase of $\Delta\theta$ plays qualitatively a similar role as a decrease of temperature with respect to the emergence of new facets of higher GB energy.

These investigations were partly supported by German Federal Ministry for Education and Research (WTZ-Project RUS 04/014), INTAS (contract 03-51-3779), Russian Foundation for Basic Research RFBR (contract 04-03-32800) and NATO Linkage grant (contract PST.CLG.979375). Fruitful discussions with Profs. E. Rabkin and W. Gust, Dr. S. Protasova, and Dr. W. Sigle are acknowledged.

References

[1] H. Minoda: Thin Solid Films 424 (2003) 40.
[2] S.B. Lee, D.Y. Yoon, M.F. Henry: Acta mater. 48 (2000) 3071.
[3] R. Hild, C. Seifert, M. Kammler, F.J. Meyer zu Heringdorf, M. Horn-von-Hoegen, R.A. Zhachuk, B.Z. Olshanetsky: Surf. Sci. 512 (2002) 117.
[4] B.B. Straumal, V.G. Sursaeva, S.A. Polyakov: Interface Sci. 9 (2001) 275.
[5] A.A. Baski, K.M. Saoud, K.M. Jones: Appl. Surf. Sci. 182 (2001) 216.
[6] J.S. Choi, D.Y. Yoon: ISIJ International 41 (2001) 478.
[7] C.W. Park, D.Y. Yoon, J.E. Blendell, C.A. Handwerker: J. Amer. Ceramic Soc. 86 (2003) 603.
[8] B.B. Straumal, L.S. Shvindlerman: Acta metall. 33 (1985) 1735.
[9] E.L. Maksimova, L.S. Shvindlerman, B.B. Straumal: Acta metall. 36 (1988) 1573.
[10] A.A. Zisman, V.V. Rybin: Poverkhnost' 7 (1982) 87 (in Russian).
[11] B.B. Straumal, S.A. Polyakov, E. Bischoff, W. Gust, E.J. Mittemeijer: Interf. Sci. 9 (2001) 287.
[12] G.D. Sukhomlin, A.V. Andreeva: phys. stat. sol. a 78 (1983) 333.
[13] J. Schöllhammer, B. Baretzky, W. Gust, E. Mittemeijer, B. Straumal: Interf. Sci. 9 (2001) 43.

[14] J. Schöllhammer, L.-S. Chang, E. Rabkin, B. Baretzky, W. Gust, E.J. Mittemeijer: Z. Metallkd. 90 (1999) 687.
[15] J.M. Pénisson, U. Dahmen, M.J. Mills: Phil. Mag. Lett. 64 (1991) 277.
[16] P.J. Goodhew, T.Y. Tan, R.W. Balluffi: Acta metall. 26 (1978) 557.
[17] F.D. Tichelaar, F.W. Schapink: J. Phys. Paris 49-C5 (1988) 293.
[18] A. Bourret, J.J. Bacmann: Inst. Phys. Conf. Series 78 (1985) 337.
[19] T. Muschik, W. Laub, M.W. Finnis, W. Gust: Z. Metallkd. 84 (1993) 596.
[20] A. Barg, E. Rabkin, W. Gust: Acta metall. mater. 43 (1995) 4067.
[21] U. Wolf, F. Ernst, T. Muschik, M.W. Finnis, H.F. Fischmeister: Phil. Mag. A 66 (1992) 991.
[22] F. Ernst, M.W. Finnis, D. Hofmann, T. Muschik, U. Schönberger, U. Wolf: Phys. Rev. Lett. 69 (1992) 620.
[23] D. Hofmann, M.W. Finnis: Acta metall. mater. 42 (1994) 3555.
[24] J.W. Matthews: Scripta Metall. 11 (1977) 233.
[25] A.P. Sutton, R.W. Balluffi: Interfaces in crystalline materials, Clarendon press, Oxford (1995).
[26] W.T. Read, W. Shockley: Phys. Rev. 78 (1950) 275.
[27] W.T. Read: Dislocations in crystals, McGraw Hill, New York (1953).
[28] C. Herring: Phys. Rev. 82 (1951) 87.
[29] C. Rottman, M. Wortis: Phys. Rev. B 24 (1981) 274.
[30] C. Rottman, M. Wortis: Phys. Rev. B 29 (1984) 328.
[31] G. Wulff: Trudy Warsh. obsh. estestvoisp. 6 (1894) 7 (in Russian).
[32] G. Wulff: Zeitschrift f. Krystallogr. 34 (1901) 449 (in German).
[33] J.D. Weeks, in: T. Riste (Ed.), Ordering in strongly fluctuating condensed matter systems, Plenum, New York (1980) 293.
[34] L.D. Landau, E.M. Lifshitz: Statistical Physics, Pergamon, Oxford (1980).
[35] V.I. Marchenko: Sov. Phys. JETP 54 (1981) 605.
[36] J.C. Heyraud, J.J. Metois: Acta Metall. 28 (1980) 789.
[37] J.C. Heyraud, J.J. Metois: J. Cryst. Growth 50 (1980) 571.
[38] J.C. Heyraud, J.J. Metois: Surf. Sci. 128 (1983) 334.
[39] R. Wagner, S.C. Steel, O.A. Andreeva, R. Jochemsen, G. Frossati: Phys. Rev. Lett. 76 (1996) 263.
[40] C. Rottman, M. Wortis, J.C. Heyraud, J.J. Metois: Phys. Rev. Lett. 52 (1984) 1009.
[41] Y. Carmi, S.G. Lipson, E. Polturak: Phys. Rev. B 36 (1987) 1894.

(Received June 5, 2004; accepted July 3, 2004)

Correspondence address

Prof. Dr. Boris Straumal
Institute of Solid State Physics, Russian Academy of Sciences
Chernogolovka, 142432 Russia
Tel.: +7 916 676 8673
Fax: +7 095 238 2326
E-Mail: straumal@issp.ac.ru; straumal@song.ru